*mathematics*

MDPI

*Article*

# Most Probable Dynamics of the Single-Species with Allee Effect under Jump-Diffusion Noise

**Almaz T. Abebe [1], Shenglan Yuan [2,*], Daniel Tesfay [3] and James Brannan [4]**

[1] Department of Mathematics, College of Art and Science, Howard University, Washington, DC 20059, USA; almaz.abebe@howard.edu
[2] Department of Mathematics, School of Sciences, Great Bay University, Dongguan 523000, China
[3] Department of Mathematics, Mekelle University, Mekelle P.O. Box 231, Ethiopia; daniel.tesfay@mu.edu.et
[4] Department of Mathematical Sciences, Clemson University, Clemson, SC 29634, USA; jrbrn@clemson.edu
* Correspondence: shenglanyuan@gbu.edu.cn

**Abstract:** We explore the most probable phase portrait (MPPP) of a stochastic single-species model incorporating the Allee effect by utilizing the nonlocal Fokker–Planck equation (FPE). This stochastic model incorporates both non-Gaussian and Gaussian noise sources. It has three fixed points in the deterministic case. One is the unstable state, which lies between the two stable equilibria. Our primary focus is on elucidating the transition pathways from extinction to the upper stable state in this single-species model, particularly under the influence of jump-diffusion noise. This helps us to study the biological behavior of species. The identification of the most probable path relies on solving the nonlocal FPE tailored to the population dynamics of the single-species model. This enables us to pinpoint the corresponding maximum possible stable equilibrium state. Additionally, we derive the Onsager–Machlup function for the stochastic model and employ it to determine the corresponding most probable paths. Numerical simulations manifest three key insights: (i) when non-Gaussian noise is present in the system, the peak of the stationary density function aligns with the most probable stable equilibrium state; (ii) if the initial value rises from extinction to the upper stable state, then the most probable trajectory converges towards the maximally probable equilibrium state, situated approximately between 9 and 10; and (iii) the most probable paths exhibit a rapid ascent towards the stable state, then maintain a sustained near-constant level, gradually approaching the upper stable equilibrium as time goes on. These numerical findings pave the way for further experimental investigations aiming to deepen our comprehension of dynamical systems within the context of biological modeling.

**Keywords:** single-species model; most probable phase portrait; jump-diffusion processes; Onsager–Machlup function; extinction probability

**MSC:** 39A50; 45K05; 65N12

check for updates

**Citation:** Abebe, A.T.; Yuan, S.; Tesfay, D.; Brannan, J. Most Probable Dynamics of the Single-Species with Allee Effect under Jump-Diffusion Noise. *Mathematics* **2024**, *12*, 1377. https://doi.org/10.3390/math12091377

Academic Editor: Ivo Siekmann

Received: 20 March 2024
Revised: 29 April 2024
Accepted: 29 April 2024
Published: 30 April 2024



## 1. Introduction

Single-species dynamics is one of the core research areas in theoretical ecology. Research about single-species dynamics enables the researcher to find out the conditions of extinction and persistence of the species. The researchers' strong motivation to develop mathematical models is to understand the underlying causes of cyclical patterns, such as those observed in population dynamics of stochastic single-species models [1].

Population modeling is very important for species management, for example, in developing recovery plans for species threatened by extinction, managing fisheries for the highest possible sustainable yield, and trying to contain or prevent the spread of invasive species [2–4].

The biological phenomenon of the Allee effect occurs when the per capita growth rate of a population decreases and the population size becomes significantly low. This is a thorough biological explanation of the Allee effect that can be due to various factors,

such as difficulties in finding resources, decreased mating opportunities, or even increased predation risk. Incorporating the Allee effect into the model is crucial in capturing these dynamics, especially when modeling endangered species or those at risk of extinction. In the literature, one can find several models of the dynamical single-species growth system; the Gompertz growth model [5], Verhulst growth model with or without Allee effect [6], power law growth model [7], interconnections between deterministic and stochastic systems [8], and Gilpin–Ayala model [9] are only a few that can be mentioned.

Outside of a few clear trends, the dynamics of biological phenomena, particularly of populations for living beings, are frequently influenced by unpredictable components due to the complexity and variability of environmental conditions [10]. Researchers have been extensively studying biological dynamical systems for a long time now, particularly in the context of modeling and analyzing random fluctuations [11,12]. The study of population events such as persistence in stationary distribution and extinction in stochastic single-species models has become an interesting and important research field. Developing the sufficient conditions for the persistence of biological species is one of the hot issues in population dynamics, as mentioned in [13–15] and references therein.

The population may be affected by sudden environmental noise [16,17]. For example, earthquakes [18], changes in temperature [19], and hurricanes [20] can be appropriately modeled as random fluctuations or stochastic events, as their occurrence and impact are less predictable and more influenced by stochasticity. These sudden environmental perturbations may bring substantial social and economic losses. Stochastic single-species models perturbed by Brownian motion have been extensively researched by many scholars [21–26]. However, stochastic extension of population process driven by Gaussian noise cannot explain the aforementioned random and intermittent environmental perturbations. Introducing a Lévy process into the underlying population dynamics would explain the impact of these random jumps. There have been a few studies investigating dynamical systems where the noise source is a Lévy process [27]. Implying the Lévy noise in the biological system to simulate the effect caused by the external environment is more effective and nearer to reality than using Gaussian noise. The investigation of the single-species model is still in its infancy, even though noisy fluctuations naturally portray random intermittent jumps. Lévy noise is widely applied in studying natural and man-made phenomena in science, among which we can mention biology [28], physics [29], and economics [30].

Under this research heading, we consider the population dynamics of a single-species growth model with Allee effect perturbed by stable Lévy fluctuations. We analyze the influence of Lévy noisy fluctuation on System (1). Investigating the impact of noisy fluctuations plays a pivotal part in demonstrating the intricate interactions between single-species models and their complex surroundings. We study how Allee effects and stochasticity affect the population persistence together.

The most probable phase portrait was first proposed by Duan [31] (Section 5.3.3). Cheng et al. [32] obtained the analytical results of the MPPP and showed that the MPPP can provide useful information about the propagation of stochastic dynamics in a one-dimensional model. Wang et al. [33] studied stochastic bifurcation by applying the qualitative changes of the MPPP to a stochastic system driven by multiplicative stable Lévy noise. In [34], the authors investigated the most probable trajectories of the tumor growth system with immune surveillance under correlated Gaussian noises and derived the analytical solution of the most probable steady state by utilizing the extremum theory with the local Fokker–Planck equation for the system. A function which summarizes the behavior of the dynamics of a continuous stochastic process was defined as the Onsager–Machlup function [35]. The Onsager–Machlup function for stochastic models driven by both non-Gaussian and Gaussian noises was established in [36]. The authors also examined the corresponding MPPP of the stochastic dynamical systems. Cheng et al. [37] focused on the impact of Gaussian noise and jump-stable Lévy noise in a genetic regulatory system; they minimized the Onsager–Machlup action functional for the stochastic dynamics driven by

Gaussian noise and obtained the most probable transition pathway. This inspired us to study the MPPP of the single-species model.

Therefore, our goal involves investigating how the most probable trajectories escape from the single-species state to the extinction state more quickly. This investigation can contribute to answering critical questions in the field of biology. Among these, it is important to answer the question of whether there exists a transition between permanence and extinction. We probe the transition pathways from the extinction state to the stable state, which are crucial in a single-species model. This allows us to investigate the biological behavior of species.

To the best of our knowledge, the work in [38] is closely related to our work; Y. Jin employed a Lévy jump process to describe sudden environmental perturbations and developed a stochastic model for a single species incorporating both the Allee effect and jump-diffusion. She demonstrated that this model possesses a unique, global, and positive solution; furthermore, she examined the stochastic permanence, extinction, and growth rate of the solution, discovering that these properties are intricately linked to the jump-diffusion component of the model.

However, our results in the present paper are different from those in [38]. We delve into the most probable phase portrait of a stochastic single-species model that incorporates the Allee effect and is influenced by both non-Gaussian and Gaussian noise. The deterministic counterpart of this model exhibits three fixed points, with one being an unstable state sandwiched between two stable equilibria. We derive the Onsager–Machlup function for the stochastic model and proceed to determine the most probable paths that it follows. Additionally, we conduct numerical simulations to corroborate our theoretical findings.

Gao et al. [39] proposed a fast and accurate numerical algorithm to simulate the nonlocal Fokker–Planck equations with non-Gaussian $\alpha$-stable symmetric Lévy motions, whether on a bounded or infinite domain. Compared with this paper, the connection is that we utilize a finite difference method, which they have also explored, to find numerical solutions for the Fokker–Planck equation determined by a nonlocal differential equation. The difference lies in that we obtain the maximum possible path of the population system in the single-species model under jump-diffusion noise and determine the corresponding maximum possible stable equilibrium state.

In this study, we compute a single-species model, concentrating on the Verhulst growth model with the Allee effect developed by Y. Jin [38]. Explicitly, we consider the following stochastic single-species growth model with Allee effect:

$$dX_t = X_{t-}\left[\left(s - \gamma_2 X_{t-} - \frac{\gamma_3}{\gamma_3 \gamma_4 X_{t-} + 1}\right)dt + \lambda dB_t + \int_{\mathbb{Y}} \epsilon(y)\tilde{N}(dt, dy)\right] \tag{1}$$

for $t \geq 0$ and $X_0 = x_0$, where $X_{t-}$ is the left limit of the population size $X_t$. A detailed description of parameters reflecting biological mechanisms is outlined in Table 1.

**Table 1.** Biological meaning of the parameters and variables in the single-species Model (1).

| Parameter | Definition |
|---|---|
| $s$ | The growth rate |
| $\gamma_2$ | The intraspecific competition rate |
| $\gamma_3$ | The attack rate |
| $\gamma_4$ | The handling time of predator |
| $M = s/\gamma_2$ | The carrying capacity |
| $t$ | Time |

Model (1) should be computationally efficient, allowing for fast simulations and analysis. It is important for Model (1) to capture essential biological details; however, over-complicating the model can make it more difficult to interpret and validate. Finding the right balance between simplicity and complexity is crucial. Model (1) is applicable to the specific biological system, organism, tissue, or cellular process of interest.

The stochastic force $\tilde{N}(dt, dy) = N(dt, dy) - \nu_\alpha(dy)dt$ is a compensated Poisson random measure with associated Poisson random measure $N(dt, dy)$ and intensity measure $\nu_\alpha(dy)dt$, in which $\nu_\alpha(dy)$ is a Lévy measure on a measurable subset $\mathbb{Y}$ of $(0, \infty)$ with $\nu_\alpha(\mathbb{Y}) < \infty$.

It is important to acknowledge the need to balance biological realism with mathematical tractability. The following restriction on System (1) is natural for biological meaning:

$$1 + \epsilon(y) > 0, \quad y \in \mathbb{Y};$$

when $\epsilon(y) > 0$, the perturbation stands for the increasing species, e.g., planting, while $\epsilon(y) < 0$ represents that the species is decreasing, e.g., harvesting and epidemics.

The main aim of this study is to investigate the stochastic dynamics of single-species biological populations in random environments. We model the evolution of these populations with first-order ordinary autonomous differential equations by introducing the coefficients and inputs, which are stochastic processes. The two stochastic processes germane to this study are Brownian motion and Lévy process. Brownian motion describes random fluctuations that are continuous in time but nowhere differentiable (see Section 2.1); a Lévy process, of which Brownian motion is a special case, is used to model random fluctuations that may have discontinuities or jumps (see Section 2.2).

Here, we develop a stochastic single-species model with the Allee effect influenced by Gaussian and non-Gaussian noises. Model (1) accurately captures the essential biological processes. In other words, the model is relevant and suitable for investigating the specific aspects of biology under consideration. First, we review the deterministic version of the model, calculate its equilibrium solutions, and describe the behavior of the fixed points. Second, we obtain the highest possible paths and the corresponding maximum possible stable states attracting the nearby maximum possible paths of the stochastic System (1). We accomplish this by finding the stationary density function, which is the solution of the nonlocal Fokker–Planck equation. To solve the nonlocal partial differential equation, we use the finite difference method proposed in [39]. This method helps us explore to some dynamical behaviors of the single-species system under the impact of non-Gaussian Lévy noise.

The rest of this study is organized as follows. In Section 2, we recall the definitions of the one-dimensional Brownian motion $B_t$ and symmetric $\alpha$-stable Lévy motion $L_t^\alpha$. In Section 3, we discuss the formulation and analysis of the deterministic single-species Model (2) the with Allee effect. In Section 4, we explain the analysis of the stochastic single-species Model (1) with Allee effect. We then review the definition of the Onsager–Machlup function and most probable phase portraits in Sections 4.1 and 4.2, respectively. The numerical results and the biological implication of our experimental findings are presented in Section 5. We conclude our research with a brief summary in the last section.

## 2. Preliminaries

In this section, we define the one-dimensional Brownian motion starting at time $t = 0$ as a process $B_t$ and $\alpha$-stable Lévy motion $L_t^\alpha$, which constitute a class of stochastic processes that have independent and stationary increments as defined below. Throughout this study, we denote $\mathbb{R}^+ = [0, \infty)$, $\mathbb{R} = (-\infty, \infty)$, and $X_t \in \mathbb{R}^+$ for $t \geq 0$.

### 2.1. Brownian Motion

Brownian motion $B_t$ (also called Wiener process) is a one-dimensional stochastic process defined on the complete probability space $(\Omega, \mathcal{F}, \mathcal{F}_t, \mathbb{P})$, which has independent and stationary increments. Brownian motion $B_t$ satisfies the following conditions:

(i) The process starts at the origin, i.e., $B_0 = 0$ almost surely;
(ii) $B_t$ has independent increments, i.e., $B_t - B_s$ is independent of the past $B_u - B_v$ for $0 \leq v < u < s < t$;
(iii) $B_t$ has stationary increments, i.e., $B_t - B_s \sim B_{t-s}$ is normally distributed with mean 0 and variance $t - s$ for any $0 \leq s \leq t$;
(iv) $B_t$ has continuous paths, and its paths are nowhere differentiable almost surely.

### 2.2. The α-Stable Lévy Motion

Lévy motions $L_t$ are a class of non-Gaussian stochastic processes. A Lévy motion $L_t$ having values in $\mathbb{R}$ is determined by a drift coefficient $\hat{b} \in \mathbb{R}$, $\hat{Q} \geq 0$ and a Borel measure $\nu$ defined on $\mathbb{R} \setminus \{0\}$. The triplet $(\hat{b}, \hat{Q}, \nu)$ is the so-called generating triplet of Lévy motion $L_t$. A Lévy motion can be written as a linear combination of time $t$, a Brownian motion, and a pure jumping process, i.e., $L_t$ can be expressed as the Lévy–Itô decomposition

$$L_t = \hat{b}t + B_{\hat{Q}}(t) + \int_{|y|<1} y\tilde{N}(t, dy) + \int_{|y|\geq 1} yN(t, dy),$$

where $N(t, dy)$ is the independent Poisson random measure on $\mathbb{R}^+ \times \mathbb{R} \setminus \{0\}$, $\tilde{N}(t, dy) = N(t, dy) - \nu(dy)dt$ is the compensated Poisson random measure, $\nu(S) = \mathbb{E}(N(1, S))$ is the jump measure, and $B_{\hat{Q}}(t)$ is the independent Brownian motion.

The Lévy–Khinchin formula for Lévy motion has a specific form of its characteristic function

$$\mathbb{E}[e^{(i\,\xi L_t)}] = e^{t\phi(\xi)}, \quad 0 \leq t < \infty,$$

where

$$\phi(\xi) = i\,\xi\hat{b} - \frac{\hat{Q}}{2}\xi^2 + \int_{\mathbb{R}\setminus\{0\}} (e^{i\,\xi z} - 1 - i\,\xi z \mathbb{1}_{|z|<1})\nu(dz), \quad \xi \in \mathbb{R}.$$

A stable distribution $S_\alpha(\theta, \beta, \gamma)$ is the distribution for a stable random variable, where the stability index $\alpha \in (0, 2)$, the skewness $\beta \in (0, \infty)$, the shift $\gamma \in (-\infty, \infty)$, and scale index $\theta \geq 0$. An $\alpha$-stable Lévy motion $L_t^\alpha$ is a non-Gaussian stochastic process satisfying

(i) $L_0^\alpha = 0$, almost surely;
(ii) The random variables $L_{t_{i+1}}^\alpha - L_{t_i}^\alpha$ are independent for $0 \leq t_1 < t_2 < \cdots < t_{i-1} < t_i < t_{i+1} < \infty$ and for each $i = 1, 2, \cdots$;
(iii) $L_t^\alpha - L_s^\alpha$ and $L_{t-s}^\alpha$ have the same distribution $S_\alpha((t-s)^{1/\alpha}, 0, 0)$;
(iv) $L_t^\alpha$ has stochastically continuous sample paths, i.e., for $0 \leq s \leq t$ and $\delta > 0$, the probability $\mathbb{P}(|L_t^\alpha - L_s^\alpha| > \delta)$ approaches zero as $t \to s$.

In the case of a one-dimensional isotropic $\alpha$-stable Lévy motion, the Lévy triplet has the drift factor $\hat{b} = 0$ and diffusion coefficient $\hat{Q} = 0$. In this study, we focus on a jump process with a specific size in generating the triplet $(0, 0, \nu_\alpha)$ for the random distribution $S_\alpha$, which can be defined by $\Delta L_t^\alpha = L_t^\alpha - L_{t-}^\alpha < \infty,\ t \geq 0$ (where $L_{t-}^\alpha$ is the left limit of the $\alpha$-stable Lévy motion in $\mathbb{R}$ at any time $t$). Here, $\nu_\alpha(dz) = c(\alpha)\frac{1}{|z|^{1+\alpha}}dz$ is Lévy measure with $c_\alpha = \alpha\frac{\Gamma(\frac{1+\alpha}{2})}{2^{1-\alpha}\pi^{\frac{1}{2}}\Gamma(1-\frac{\alpha}{2})}$ and $\Gamma$ is the Gamma function.

**Remark 1.** *Condition (iv) of α-stable Lévy motion is equivalent to the following way: $t \mapsto L_t^\alpha$ is a.s. càdlàg up to a modification of the process. A special case of α-stable Lévy motion is Brownian motion when α = 2. The Poisson process, α-stable process, compound Poisson process, etc., are also examples of Lévy processes.*

## 3. Dynamical Analysis of the Deterministic Model

The deterministic form of the nonlinear Model (1) without noise is provided as

$$\frac{dX_t}{dt} = X_t\left(s - \gamma_2 X_t - \frac{\gamma_3}{\gamma_3\,\gamma_4\,X_t + 1}\right) =: F(X_t), \quad t \geq 0, \quad X_0 = x_0. \tag{2}$$

This system can be written as $\frac{dX}{dt} = -\frac{dU(X)}{dX}$, where $U(X)$ is the potential function provided by

$$U(X) := -\frac{s\,X^2}{2} + \frac{\gamma_2\,X^3}{3} + \frac{\gamma_3}{(\gamma_3\,\gamma_4)^2}[\gamma_3\,\gamma_4\,X + 1 - \ln(\gamma_3\,\gamma_4\,X + 1)].$$

The single-species Model (2) with Allee effect has equilibrium points $X_1 = 0$ and

$$\begin{aligned} X_{2,3} &= \frac{(s\gamma_3\gamma_4 - \gamma_2) \pm \sqrt{(s\gamma_3\gamma_4 - \gamma_2)^2 - 4\gamma_2\gamma_3\gamma_4(\gamma_3 - s)}}{2\gamma_2\gamma_3\gamma_4} \\ &= \frac{(s\gamma_3\gamma_4 - \gamma_2) \pm (s\gamma_3\gamma_4 - \gamma_2)\sqrt{1-\beta}}{2\gamma_2\gamma_3\gamma_4} \\ &= \frac{(s\gamma_3\gamma_4 - \gamma_2)\left(1 \pm \sqrt{1-\beta}\right)}{2\gamma_2\gamma_3\gamma_4}, \end{aligned}$$

where $\beta = \frac{4\gamma_2\gamma_3\gamma_4}{(s\gamma_3\gamma_4 - \gamma_2)^2}(\gamma_3 - s)$. If $\beta < 1$, then the equilibrium states of System (2) are:

$$\begin{aligned} &X_1 = 0, \quad \text{an extinction equilibrium;} \\ &X_2 = \frac{(s\gamma_3\gamma_4 - \gamma_2)\left(1 - \sqrt{1-\beta}\right)}{2\gamma_2\gamma_3\gamma_4}, \quad \text{a lower unstable equilibrium;} \\ &X_3 = \frac{(s\gamma_3\gamma_4 - \gamma_2)\left(1 + \sqrt{1-\beta}\right)}{2\gamma_2\gamma_3\gamma_4}, \quad \text{an upper stable equilibrium.} \end{aligned}$$

If $\beta = 1$, then the equilibria $X_2$ and $X_3$ collide. The single-species deterministic Model (2) has only two equilibrium states:

$$\text{stable state } X_1 = 0, \quad \text{and} \quad \text{unstable state } X_* = \frac{s\gamma_3\gamma_4 - \gamma_2}{2\gamma_2\gamma_3\gamma_4}.$$

The derivative of $F(X)$ is

$$F'(X) = s - 2\gamma_2 X - \frac{\gamma_3}{(\gamma_3\,\gamma_4\,X + 1)^2}.$$

For simplicity and convenience of discussion, we choose the parameters $\gamma_3\,\gamma_4 = 1$, $s = 1$, $0 < \gamma_2 < 1$, and $0 < \gamma_3 < \frac{(1+\gamma_2)^2}{4\gamma_2}$; therefore, $\beta = \frac{4\gamma_2(\gamma_3 - 1)}{(1-\gamma_2)^2}$ and $X_* = \frac{1-\gamma_2}{2\gamma_2}$. For $\beta < 1$, the extinction state $X_1 = 0$ and the equilibrium solution $X_3$ are stable, while $X_2$ is unstable. Figure 1b reveals that when the value of the attack rate $\gamma_3$ increases, the unstable state $X_2$ and stable state $X_3$ become closer to each other, then become one solution $X_*$, and finally disappear. This indicates the occurrence of saddle-node bifurcation.

**Remark 2.** *The reason we choose $\gamma_3\gamma_4 = 1$ is to simplify the problem. If we change this assumption, there will be no violation, because whether the equilibria $X_2$ and $X_3$ collide into $X_*$ depends on whether $\beta$ is equal to 1.*

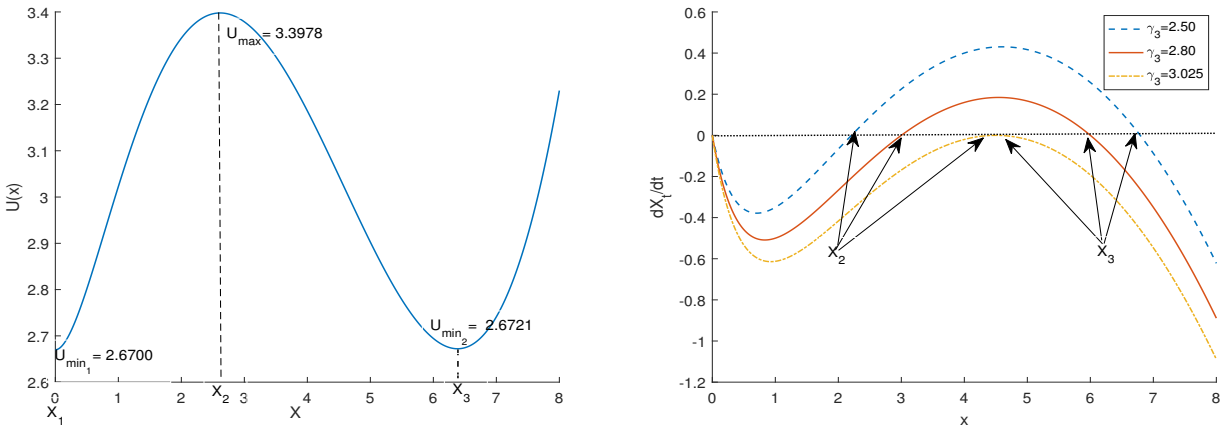


(**a**) (**b**)

**Figure 1.** (**a**) A plot of the bistable potential function $U(X)$ of the nonlinear Model (2). Dashed black lines indicate local unstable and stable equilibria at $X_2 = 2.6159$ and $X_3 = 6.3841$, respectively. (**b**) The phaselines of the single-species Model (2). Parameters: $s = 1$, $\gamma_2 = 0.1$, $\gamma_3 = 2.67$, and $\gamma_4 = \frac{1}{\gamma_3}$ in the graph of $\frac{dX}{dt}$.

The critical value of the attack rate $\gamma_c = 2.67$ of the deterministic single-species system (2) with Allee effect is obtained by solving the equation $U(X_1) = U(X_3)$. This value is an important indication of the transition phenomena between the unstable and stable states for the deterministic single-species growth model. The steady extinction state $X_1$ is stable if $\gamma_3 > \gamma_c$, and the steady state $X_3$ exhibits the stability property for $\gamma_3 < \gamma_c$.

## 4. Dynamical Analysis of the Stochastic System

In this section, we discuss the behavior of the solution of the stochastic System (1). First, we recall the definition of the Onsager–Machlup function for the stochastic differential equation (SDE) driven by jump noise. This helps to measurethe Onsager–Machlup functional induced by the jump process. Second, we examine the corresponding most probable paths. Finally, we present the findings of a numerical experiment using the finite difference method [39]. The numerical solution of the stochastic model provides useful information for understanding the dynamical behavior of the stochastic system (1).

### *4.1. Onsager–Machlup Functional*

The Onsager–Machlup functional determines a probability density for a stochastic process in which the probability density is estimated implicitly. It can be used for the purposes of reweighting and sampling trajectories as well as for determining the most probable trajectory based on variational arguments. The most probable transition pathway can be obtained by minimizing the Onsager–Machlup function. The whole procedure enables us to detect the dynamics of the most probable path [40].

As proved by Jin [38], the stochastic single-species System (1) with Allee effect has a unique global and positive solution with the initial condition $X_0 = x_0$. The jump-diffusion process $X_t$ is adapted and càdlàg (see Figure 2); when $\lambda = 0$ and $\epsilon = 0.9$, the yellow trajectory in Figure 2a shows a specific biological scenario where the Allee effect is likely to manifest. The intensity of the jump is sufficiently large that the species becomes extinct.

We denote the space of càdlàg paths starting at $x_0$ of a solution process $X = \{X_t, t \geq 0\}$ of (1) by

$$\mathcal{D}_{x_0} = \{X : \text{ for any } t \geq 0, \lim_{s \uparrow t} X_s = X_{t-}, \lim_{s \downarrow t} X_s = X_t \text{ exist and } X_0 = x_0\}.$$

This space equipped with Skorokhod's $\mathcal{J}_1$-topology generated by the metric $\mathrm{d}_{\mathbb{R}^+}$ is a Polish space [41]. For functions $x_1, x_2 \in \mathcal{D}_{x_0}$, we define

$$\mathrm{d}_{\mathbb{R}^+}(x_1, x_2) = \inf\left\{\varepsilon > 0 : |x_1(t) - x_2(\bar{\lambda}\, t)| \le \varepsilon,\ \left|\ln \frac{\arctan(\bar{\lambda}\, t) - \arctan(\bar{\lambda}\, s)}{\arctan(t) - \arctan(s)}\right| \le \varepsilon, \text{ for every } t, s \ge 0 \text{ and some } \bar{\lambda} \in \Lambda^{\mathbb{R}^+}\right\},$$

where $\Lambda^{\mathbb{R}^+} = \{\bar{\lambda} : \mathbb{R}^+ \to \mathbb{R}; \bar{\lambda} \text{ is injective increasing}, \lim_{t\to 0} \bar{\lambda}(t) = 0, \lim_{t\to\infty} \bar{\lambda}(t) = \infty\}$.

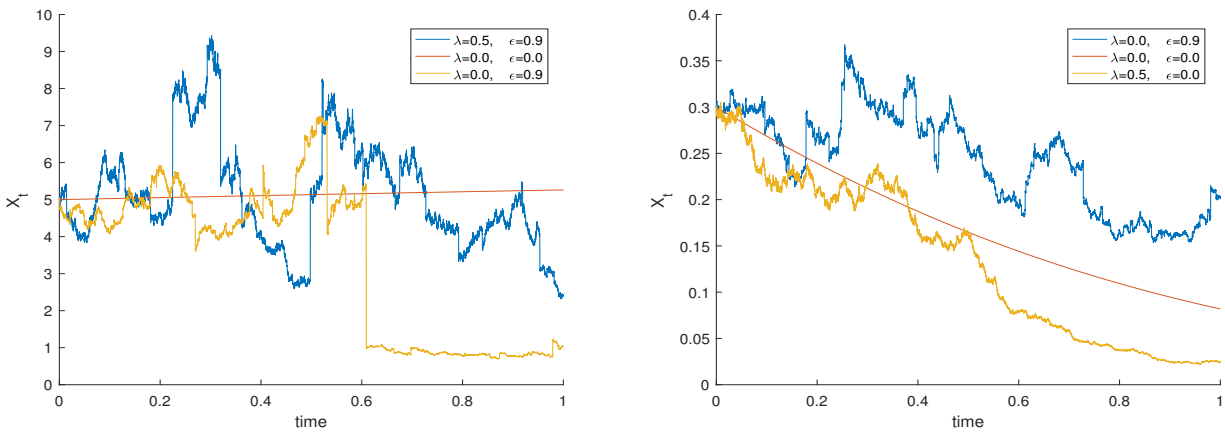


(**a**) (**b**)

**Figure 2.** The numerical simulation of System (1) when it is persistent or extinct at different value initial condition $x_0$. (**a**) Persistent sample paths of Model (1): the initial condition is $x_0 = 5$. (**b**) Extinct sample paths of Model (1) with initial condition $x_0 = 0.3$. Parameters: $s = 1$, $\gamma_2 = 0.1$, $\gamma_3 = 2.67$, $\gamma_4 = 1$, $\alpha = 1.5$, $\beta = 0.27 < 1$.

We consider the corresponding jump-diffusion process $X_t(\omega) := \omega(t), t \in [0, T]$ defined on the canonical probability space $(\mathbb{R}^{[0,T]}, \mathcal{B}(\mathbb{R})^{[0,T]}, \mathbb{P}_T)$. As the paths of $X$ are càdlàg, we identify $X_t$ on the space $(\mathcal{D}^T_{x_0}, \mathcal{B}^T_{x_0}, \mathbb{P})$ instead of $(\mathbb{R}^{[0,T]}, \mathcal{B}(\mathbb{R})^{[0,T]}, \mathbb{P}_T)$, where $\mathcal{D}^T_{x_0}$ is defined similarly as the space $\mathcal{D}_{x_0}$ on the time interval $[0, T]$. The associated Borel $\sigma$-algebra is $\mathcal{B}^T_{x_0} = \mathcal{B}(\mathbb{R})^{[0,T]} \cap \mathcal{D}^T_{x_0}$, and $(\mathcal{D}^T_{x_0}, \mathcal{B}^T_{x_0})$ is then a separable metric space. The probability measure $\mathbb{P}$ is generated by $\mathbb{P}(A \cap \mathcal{D}^T_{x_0}) := \mathbb{P}_T(A)$ for each $A \in \mathcal{B}(\mathbb{R})^{[0,T]}$. Because every càdlàg function on $[0, T]$ is bounded, we equip $\mathcal{D}^T_{x_0}$ with the uniform norm

$$\|x\| = \sup_{t\in[0,T]} |x(t)|, \quad x(t) \in \mathcal{D}^T_{x_0},$$

hence, $\mathcal{D}^T_{x_0}$ is a Banach space. In order to find the most probable tube of $X_t$, we should determine the probability that the paths lie within the closed tube

$$K(z, \varepsilon) = \{x \in \mathcal{D}^T_{x_0} : \| x - z \| \le \varepsilon,\ z \in \mathcal{D}^T_{x_0},\ \varepsilon > 0\}, \tag{3}$$

which is a subset of the space $\mathcal{D}^T_{x_0}$ of càdlàg functions on the interval from 0 to $T$ containing a function $z$ together with its $\varepsilon$-neighborhood. We define the measure $\mu_X$ on $\mathcal{B}(\mathbb{R})^{[0,T]}$ induced by the solution process $X_t$ for the stochastic nonlinear Model (1) via

$$\mu_X(B) = \mathbb{P}(\{w : X_t(\omega) \in B\}), \quad \text{for } B \in \mathcal{B}(\mathbb{R})^{[0,T]}.$$

For sufficiently small $\varepsilon > 0$, the main contribution of the above probability is provided by the measure of the trajectories in the $\varepsilon$-tube of $z \in \mathcal{D}^T_{x_0}$:

$$\mu_X(K(z, \varepsilon)) = \mathbb{P}(\{w : X_t(\omega) \in K(z, \varepsilon)\}), \tag{4}$$

where $K(z,\varepsilon) \in \mathcal{B}(\mathbb{R})^{[0,T]}$. As the $\varepsilon$-tube $K(z,\varepsilon)$ depends on the reference path $z$, it is necessary for us to look for the "most probable" trajectory $z$ which maximizes the measure $\mu_X(K(z,\varepsilon))$ in Equation (4). When we focus on the differentiable functions $z \in \mathcal{D}^T_{x_0}$, we have the following meaningful definition.

**Definition 1.** *Let $0 < \varepsilon \ll 1$ be given. For an $\varepsilon$-tube surrounding a reference path $z(t)$, the probability of the solution process $X_t, t \in [0,T]$ lying in this tube is estimated by*

$$\mathbb{P}(\| X - z \| \leq \varepsilon) \propto C(\varepsilon) \exp\left\{ -\frac{1}{2} \int_0^T \mathrm{OM}(\dot{z}, z) dt \right\},$$

*where the integrand $\mathrm{OM}(\dot{z}, z)$ is called the Onsager–Machlup function and $\propto$ denotes the equivalence relation for sufficiently small $\varepsilon$. The intergral $\int_0^T \mathrm{OM}(\dot{z}, z)dt$ is the Onsager–Machlup functional.*

**Remark 3.** *The Onsager–Machlup function is similar to the Lagrangian function of a dynamical system in classical mechanics, and the Onsager–Machlup functional would correspond to the action functional. In particular, for an SDE with pure jump Lévy noise, Definition 1 remains applicable and the minimizer of the Onsager–Machlup functional $\int_0^T \mathrm{OM}(\dot{z}, z)dt$ provides the most probable path for this non-Gaussian stochastic system. Moreover, the minimizer $z$ may be chosen from a more general function space.*

Our vital result about the expression of the Onsager–Machlup function for a jump-diffusion process is clearly presented in the main theorem.

**Theorem 1.** *For the stochastic nonlinear System (1) with jump measure satisfying $\int_{\mathbb{Y}} \epsilon(y)\nu_\alpha(dy) < \infty$, the Onsager–Machlup function [35] is characterized up to an additive constant by*

$$\begin{aligned} \mathrm{OM}(\dot{z}, z) = & \left[ \frac{\dot{z} - z\left(s - \gamma_2 z - \frac{\gamma_3}{\gamma_3 \gamma_4 z + 1}\right)}{\lambda z} \right]^2 + s - 2\gamma_2 z - \frac{\gamma_3}{(\gamma_3 \gamma_4 z + 1)^2} \\ & + 2 \frac{\dot{z} - z\left(s - \gamma_2 z - \frac{\gamma_3}{\gamma_3 \gamma_4 z + 1}\right)}{\lambda^2 z} \int_{\mathbb{Y}} \epsilon(y)\nu_\alpha(dy), \end{aligned}$$

*where $z \in \mathcal{D}^T_{x_0}$ is a differentiable function. The contribution of the pure jump Lévy noise to the Onsager–Machlup function is the nonlocal integral. When the jump measure is absent, we cover the Onsager–Machlup function for the case of diffusion. In terms of the Onsager–Machlup function, the measure of the tube $K(z,\varepsilon)$ defined in (3) can be approximated as follows:*

$$\mu_X(K(z,\varepsilon)) \propto \mu_{Y^c}(K(0,\varepsilon)) \exp\left\{ -\frac{1}{2} \int_0^T \mathrm{OM}(\dot{z}, z) dt \right\}$$

*where $Y^c_t$ is defined by*

$$dY^c_t = Y^c_t \left( \lambda\, Y^c_t dB_t + \int_{\mathbb{Y}} \epsilon(y) \tilde{N}(dt, dy) \right), \quad t \in [0,T].$$

The proof of Theorem 1 is provided in [36] (Theorem 4.1).

In the Gaussian noise case ($\epsilon(y) = 0$), the stochastic single-species Model (1) becomes

$$dX_t = X_t \left[ \left( s - \gamma_2 X_t - \frac{\gamma_3}{\gamma_3 \gamma_4 X_t + 1} \right) dt + \lambda dB_t \right], \quad t \geq 0, \quad X_0 = x_0. \tag{5}$$

We apply Lamperti transforms to solve the SDE driven by multiplicative noise [31] (Example 6.48). This method allows us to transform the multiplicative noise into additive noise. Numerically solving an additive-noise SDE is usually easier than solving a multiplicative-noise SDE, as in Equation (5).

We assume $g \in C^2(\mathbb{R})$ and define $Y_t = g = \ln(X_t)$. Then, the new SDE has the following form:

$$dY_t = G(Y_t)dt + \lambda\, dB_t \tag{6}$$

where

$$G(Y_t) = \left(h(X_t) - \frac{\lambda^2}{2}\right)\Big|_{X_t = \exp(Y_t)}$$

and

$$h(X_t) = s - \gamma_2\, X_t - \frac{\gamma_3}{\gamma_3\, \gamma_4\, X_t + 1}.$$

Because the most probable transition path for a stochastic single-species model is the minimizer of the Onsager–Machlup action functional, denoted by $Z_m$, it can be obtained from the following least action principle when the first variation vanishes, i.e.,

$$\delta \int_0^T \mathrm{OM}(\dot{z}, z)dt = 0,$$

where the integrand function (Onsager–Machlup function) [37] is provided by

$$\mathrm{OM}(\dot{z}, z) = \left(\frac{G(z) - \dot{z}}{\lambda}\right)^2 + \dot{G}(z). \tag{7}$$

Thus, Equation (7) satisfies the following Euler–Lagrange equation:

$$\frac{d}{dt}\frac{\partial \mathrm{OM}(\dot{z}, z)}{\partial \dot{z}} = \frac{\partial \mathrm{OM}(\dot{z}, z)}{\partial z}. \tag{8}$$

The most probable transition pathway $Z_m(t)$ of System (6) is characterized by

$$\begin{aligned} &\ddot{Z}_m(t) = \frac{\lambda^2}{2}\ddot{G}(Z_m) + \dot{G}(Z_m)\, G(Z_m), \qquad 0 < t < T, \\ &Z_m(0) = X_1, \;\; Z_m(T) = X_3. \end{aligned} \tag{9}$$

The way of determining the most probable transition paths of the stochastic dynamical System (5) is translated into solving the second-order Euler–Lagrange Equation (8) with two boundary conditions. To solve the two-point boundary value problem in Equation (9), we apply the shooting method with Newton iteration.

### *4.2. Most Probable Phase Portraits*

Suppose that the solution $X_t$ of System (1) has a conditional probability density $p(X, t|x_0, 0)$. For convenience, we drop the initial condition and simply denote it by $p(X, t)$. For the solution of the Fokker–Planck equation, the probability density function $p(X, t)$ is a surface in $(X, t, p)$-space. For a given time $t$, the maximizer $X_m(t)$ for $p(X, t)$ (i.e., $X_m(t) = \max_{X \in (0,\infty)} p(X, t)$) shows the most probable (i.e., maximum likelihood) location of this orbit at time $t$. The orbit traced out by $X_m(t)$ is called a most probable orbit starting at $x_0$. Thus, the deterministic orbit $X_m(t)$ follows the top ridge of the surface in the $(X, t, p)$-space as time goes on.

Nonlocal Fokker–Plank Equation

The Fokker–Planck equation describes the time evolution of the probability density function; however, it can be solved analytically only in special cases. Here, we are interested in the steady-state probability distribution (equilibrium distribution) and want to express the stationary solution of the nonlocal Fokker–Planck equation. This makes estimating of the most probable phase portrait in the Lévy noise case possible both numerically and algorithmically.

Let $f : \mathbb{R} \to \mathbb{R}$ be a smooth function. On the one hand,

$$\mathbb{E}f(X_t) = \int_{\mathbb{R}} f(X)p(X,t)dX,$$

thus,

$$\frac{d}{dt}\mathbb{E}f(X_t) = \int_{\mathbb{R}} f(X)\frac{\partial}{\partial t}p(X,t)dX;$$

on the other hand, by virtue of Itô's formula,

$$\begin{aligned} df(X_t) =& X_{t-}\left(s - \gamma_2 X_{t-} - \frac{\gamma_3}{\gamma_3\gamma_4 X_{t-} + 1}\right)f'(X_t)dt \\ &+ \int_{\mathbb{Y}} \left(f(X_t + \epsilon(y)X_{t-}) - f(X_t) - \epsilon(y)X_{t-}f'(X_t)\right)\nu_\alpha(dy)dt. \end{aligned} \tag{10}$$

Taking the expectation on both sides of (10), we obtain

$$\begin{aligned} d\mathbb{E}f(X_t) =& \mathbb{E}\Big[X_{t-}\left(s - \gamma_2 X_{t-} - \frac{\gamma_3}{\gamma_3\gamma_4 X_{t-} + 1}\right)f'(X_t)dt \\ &+ \int_{\mathbb{Y}} \left(f(X_t + \epsilon(y)X_{t-}) - f(X_t) - \epsilon(y)X_{t-}f'(X_t)\right)\nu_\alpha(dy)dt\Big]. \end{aligned} \tag{11}$$

Noting that the infinitesimal generator of the solution $X_t$ for System (1) is

$$\begin{aligned} Ap(X,t) =& X\left(s - \gamma_2 X - \frac{\gamma_3}{\gamma_3\gamma_4 X + 1}\right)\partial_X p(X,t) \\ &+ \int_{\mathbb{Y}} \left(f(X + \epsilon(y)X) - f(X) - \epsilon(y)X\partial_X p(X,t)\right)\nu_\alpha(dy). \end{aligned}$$

Equation (11) is rewritten as

$$\begin{aligned} \frac{d}{dt}\mathbb{E}f(X_t) =& \mathbb{E}\Big[X_{t-}\left(s - \gamma_2 X_{t-} - \frac{\gamma_3}{\gamma_3\gamma_4 X_{t-} + 1}\right)f'(X_t) \\ &+ \int_{\mathbb{Y}} \left(f(X_t + \epsilon(y)X_{t-}) - f(X_t) - \epsilon(y)X_{t-}f'(X_t)\right)\nu_\alpha(dy)\Big] \\ =& \int_{\mathbb{R}} \Big[X\left(s - \gamma_2 X - \frac{\gamma_3}{\gamma_3\gamma_4 X + 1}\right)f'(X) \\ &+ \int_{\mathbb{Y}} \left(f(X + \epsilon(y)X) - f(X) - \epsilon(y)X f'(X)\right)\nu_\alpha(dy)\Big]p(X,t)dX. \end{aligned} \tag{12}$$

As a result, the Fokker–Planck equation for the stochastic nonlinear System (1) of the solution process $X = \{X_t, t \geq 0\}$ with initial condition $p(X,0) = \sqrt{\frac{40}{\pi}}e^{-40(X-x_0)^2}$ is

$$\begin{aligned} \partial_t p(X,t) =& -\left(s - 2\gamma_2 X - \frac{\gamma_3}{(\gamma_3\gamma_4 X + 1)^2}\right)p(X,t) - X\left(s - \gamma_2 X - \frac{\gamma_3}{\gamma_3\gamma_4 X + 1}\right)\partial_X p(X,t) \\ &+ \int_{\mathbb{Y}} \left(f(X + \epsilon(y)X) - f(X) - \epsilon(y)X f'(X)\right)\nu_\alpha(dy)p(X,t). \end{aligned} \tag{13}$$

To simulate the nonlocal Fokker–Planck Equation (13), we apply the numerical finite difference method provided in Gao et al. [39].

If the Lévy motion is replaced by Brownian motion, then the local Fokker–Planck equation has the following form:

$$\partial_t p(X,t) = -\partial_X\left[X\left(s - \gamma_2 X - \frac{\gamma_3}{\gamma_3\gamma_4 X + 1}\right)p(X,t)\right] + \frac{\lambda^2}{2}\partial_{XX}\left(X^2 p(X,t)\right). \tag{14}$$

The stationary probability density function $p_s(X)$ of Equation (14) can be solved by

$$0 = -\partial_X \left[ X \left( s - \gamma_2 X - \frac{\gamma_3}{\gamma_3 \gamma_4 X + 1} \right) p_s(X) \right] + \frac{\lambda^2}{2} \partial_{XX} \left( X^2 p_s(X) \right), \tag{15}$$

or equivalently by

$$\begin{aligned} 0 &= -\left[ X \left( s - \gamma_2 X - \frac{\gamma_3}{\gamma_3 \gamma_4 X + 1} \right) p_s(X) \right] + \frac{\lambda^2}{2} \partial_X \left( X^2 p_s(X) \right), \\ \Longrightarrow \quad 0 &= \left[ X \left( s - \gamma_2 X - \frac{\gamma_3}{\gamma_3 \gamma_4 X + 1} \right) - \lambda^2 X \right] p_s(X) - \frac{\lambda^2 X^2}{2} \partial_X p_s(X). \end{aligned} \tag{16}$$

Due to the complexity of the stationary solution, we take the extrema of the stationary probability density function located at $x_s$ directly; in other words, the stationary probability density function satisfies $\partial_X(\, p_s(x_s)) = 0$. Because $p_s(x_s) \neq 0$, Equation (16) reduces to

$$X \left( s - \gamma_2 X - \frac{\gamma_3}{\gamma_3 \gamma_4 X + 1} \right) - \lambda^2 X = 0. \tag{17}$$

Because of the presence of noise with the $\lambda$ term, Equation (17) is completely different from the equilibrium state of the deterministic Model (2). The numerical solution of Equation (17) is plotted in Figure 3b.

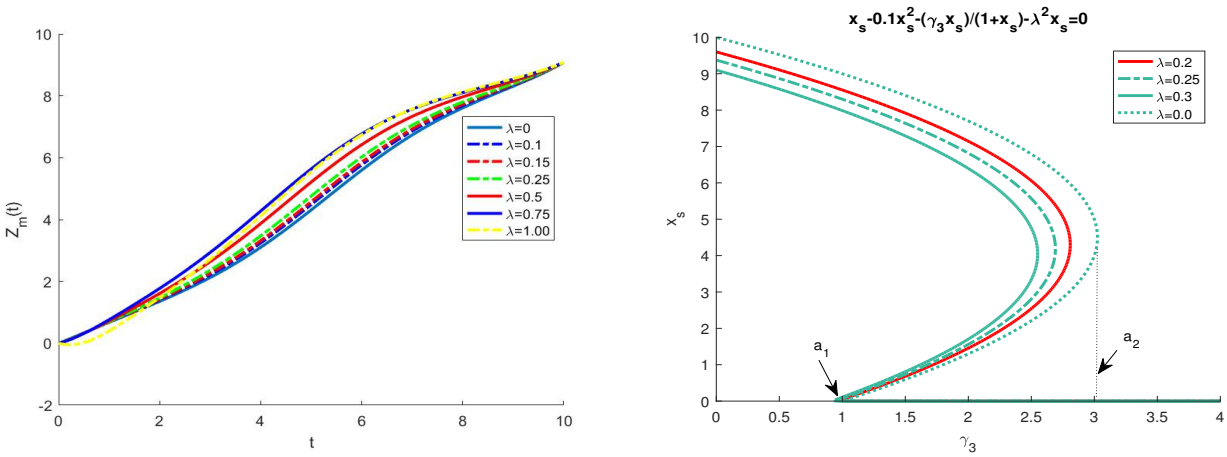


(**a**) (**b**)

**Figure 3.** (**a**) Most probable transition pathways $Z_m(t)$, starting at the extinction state $X_1 = 0$ and ending at the upper equilibrium stable state $X_3 = 9.0846$, under white noise with respect to the seven different values of $\lambda$ from 0 to 1. (**b**) The most probable steady state $x_s$ versus the attack rate $\gamma_3$ for different values of Gaussian noise intensity with $\lambda$ term.

## 5. Numerical Results and Biological Implications

To allow readers to better understand our results, we performed numerical simulations to illustrate our theoretical results. Based on the finite difference method [39], numerical simulations are very useful in the study of real population examples. In the present section, we define the bifurcation time as the time between the changes in number of maximally likely equilibrium states. This is a time scale for the birth of a new most probable stable equilibrium state. In addition, we show the intervals in which there exist one or two maximally likely stable equilibrium states, the value of the equilibrium states, and the point where the number of metastable states of the stochastic single-species Model (1) varies. Because the numerical solutions of a model depend on the values of all its deterministic parameters and noise intensities, we discuss the effect of the parameters in Table 1 on the

investigated System (1). For simplicity, we simulated the four most probable transition pathways together with the initial conditions selected in different intervals.

When plotting the figures, we fixed the deterministic parameters $s = 1$, $\gamma_2 = 0.1$, $\gamma_3 = 2.67$, $\gamma_4 = 1/\gamma_3$, the noise intensity $\epsilon = 0.5$, and the stability index $\alpha = 1.5$.

The potential function denoted by $U(X)$ in Figure 1a has two stable steady states $X_1$ and $X_3$ and an unstable steady state $X_2$ for $\beta < 1$. This function has a maximum value at the unstable equilibrium solution $X_2$. The potential function attains its minima at the stable fixed points $X_1$ and $X_3$. For the value of $\beta > 1$, the nonlinear System (2) has only one equilibrium point, which is the trivial point $X_1 = 0$.

In Figure 1b, we sketch the equilibrium states versus attack rate $\gamma_3$. For $\beta < 1$, there exist two stable equilibrium states $X_1$ and $X_3$ and one unstable equilibrium state $X_2$. While $\beta > 1$, $X_1 = 0$ is the unique equilibrium state that is stable;thus, the parameter $\beta = 1$ is the bifurcation parameter value.

The distance between the unstable equilibrium $X_2$ and the stable fixed point $X_3$ becomes very small when $\beta$ approaches 1. This indicates that the expected time to extinction may be too short, as clarified in Figure 1b.

Figure 2 displays the numerical simulation of the stochastic single-species Model (1) with Allee effect when it is persistent or extinct at different value of initial condition $x_0$. This figure proves that the solutions of the stochastic nonlinear System (1) are positive and that species extinction occurs when the initial condition is less than the value of $X_2$, as demonstrated in Figure 2b. While the initial condition is greater than the value of $X_2$, there is stochastic persistence.

In Figure 3a, we depict the most probable transition pathways $Z_m(t)$ of System (6) for seven distinct values of $\lambda$ ranging from 0 to 1. The method of finding the most probable transition paths of System (5) is equivalent to solving the one-dimensional boundary value problem in (9). A numerical technique for computing solutions of the second-order Euler–Lagrange differential in Equation (8) is the shooting method. Figure 3b demonstrates the curves for the most probable steady state $x_s$ of the stochastic single-species Model (1) with $\epsilon(y) = 0$ driven by Gaussian noise at different values of the noise intensity $\lambda$. The steady-state curves exhibit a bi-stability in the interval $(a_1, a_2)$. For $\gamma_3 > a_1$, the stable steady state stays at the extinction state, while for $\gamma_3 < a_1$ it is located at the stable equilibrium state. Because of the presence of Gaussian noise with $\lambda$ term, the numerical result in Figure 3b is completely different from the numerical result in Figure 1b. By perturbing the parameters and observing the resulting changes in model output, it is evident that Model (1) is sensitive to changes in its parameters.

Concerning the question of why the most probable transition pathways shown in Figure 3a are not related to the numerical simulations shown in Figure 2, it is because we simulated six true trajectories of the stochastic single-species Model (1) under different noise intensities in Figure 2. However, the most probable transition pathways depicted in Figure 3a are reference trajectories, which are not necessarily the true trajectories of the stochastic single-species Model (1), although their tubes are likely to contain the largest number of true trajectories of the system.

The most probable trajectories of the stochastic single-species Model (1) with Allee effect are plotted graphically in Figures 4 and 5a. Here, the values of the noise intensities are set as $\lambda = 0$ and $\epsilon = 0.5$, respectively. We choose the stability index $\alpha = 1.5$, and the interval $D = (0, 15)$. These figures evolve as the initial value $x_0$ changes, telling us that the maximal likely equilibrium state (maximizer) $X_m(t)$ lies between 9 and 10 at the bifurcation time 1.13; in other words, the maximizer in high concentration is between 9 and 10. This is different from the deterministic equilibrium stable solution $X_3 = 9.0846$ due to the effects of external noise.

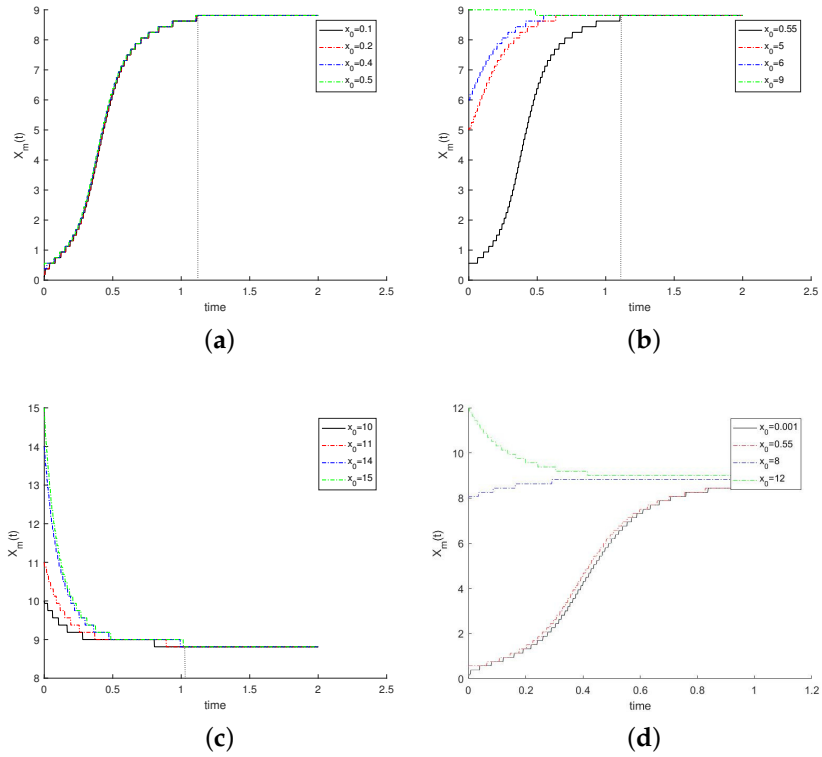


**Figure 4.** Most probable orbits and most probable equilibrium states for the stochastic nonlinear System (1) with respect to the initial condition $x_0$ and its values relative to the thresholds $X_2$ and $X_3$: (**a**) when the initial condition $x_0$ is less than the unstable equilibrium state $X_2$, i.e., $x_0 < X_2$; (**b**) when the initial condition is between $X_2$ and $X_3$, i.e., $X_2 < x_0 < X_3$; and (**c**) when the initial condition is greater than $X_3$, i.e., $x_0 > X_3$. (**d**) For the initial condition $x_0$, there is one value (0.001) which is less than $X_2$, two values (0.55 and 8) which are between $X_2$ and $X_3$, and one value (12) which is greater than $X_3$. Parameters: $s = 1$, $\gamma_2 = 0.1$, $\gamma_3 = 2.67$, $\gamma_4 = 1$, $\alpha = 1.5$, $\epsilon = 0.5$, $\beta = 0.27 < 1$, $\lambda = 0$, and bifurcation time at 1.13 (dotted vertical line).

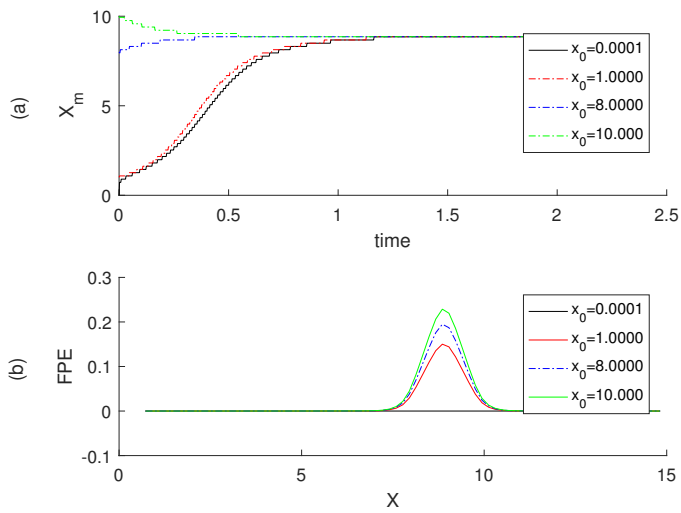


**Figure 5.** (**a**) Most probable orbits and most probable equilibrium states for System (1) with equilibrium state $X_m$ between 9 and 10. For the initial condition $x_0$, there is one value (0.0001) which is less than $X_2$, two values (1 and 8) between $X_2$ and $X_3$, and one value (10) which is greater than $X_3$. (**b**) The solution of the FPE of Model (1). The stationary density function of the FPE has its maximum value at the equilibrium state $X_m$. The other parameters are fixed: $s = 1$, $\gamma_2 = 0.1$, $\gamma_3 = 2.67$, $\gamma_4 = 1$, $\alpha = 1.5$, $\epsilon = 0.5$, $\beta = 0.27 < 1$, $\lambda = 0$, and $x_0 \in (0, 10]$. The bifurcation time is 1.13.

Figure 5a draws the MPPP for different values of the initial point $x_0$. As seen in Figure 5a, the most probable growth state is attracted to the maximally likely equilibrium state of extinction, then leads to the maximally likely equilibrium state in the high concentration as time moves forward. For the initial point $x_0$ with two values of 0.0001 and 1 around $X_2$, the two trajectories of $X_m$ starting from them are relatively close. Given two specific values 8 and 10 of the initial point $x_0$ that are around $X_3$, the ascending trajectory of $X_m$ starting from $x_0 = 8$ and the descending trajectory starting from $x_0 = 10$ coincide at a specific time point, which is 0.5.

From Figure 5b, it can be observed that the maximum value of the stationary density function $p(X,t)$ is situated at the maximum likely stable state $X_m(t) = 9.0846$ with the initial condition $p(X,0) = \sqrt{\frac{40}{\pi}}e^{-40(X-x_0)^2}$. As the initial condition $x_0$ increases, it raises the peak point of the stationary density function $p(X,t)$. This shows that the extinction of the species may not happen, and the high peak occurs at the maximum likely stable state $X_m(t)$.

When there is no jump in the stochastic single-species Model (1), i.e., $\epsilon(y) = 0$, Figure 3a illustrates the most probable transition paths in the $(Z_m, t)$-plane with initial condition $Z_m(0) = 0$ and terminal condition $Z_m(10) = 9.0846$ under the same transition time interval $t \in [0, 10]$ for different values of $\lambda$. Figure 3b displays the most probable steady state $x_s$ determined by (17) (computed by numerical simulations under $\gamma_2 = 0.1$) for different values of $\lambda$. When there exist jumps in the stochastic single-species Model (1) with $\epsilon = 0.5$ and $\lambda = 0$, we calculated the four most probable transition pathways using simulations based on the system dynamics and the given parameters, as exhibited in Figures 4 and 5a. Regardless of the starting point, these most probable transition pathways eventually converge to a specific horizontal line with $X_m$ between 9 and 10. The fact that the high peak of the stationary density function is located at 9.0846 effectively corroborates this point, as demonstrated in Figure 5b. The most probable transition pathways ultimately provide a more comprehensive understanding of the system's behavior and validate the predicted dynamics of the system through numerical simulations.

Figure 6a tells us that as time increases, the most probable paths converge quickly to the stable state $X_3$ and remain at a nearly constant level, then approach the high stable equilibrium state. Although the values of the initial point $x_0$ are different, these most probable transition pathways invariably converge towards a specific horizontal line positioned within the range of $X_m$ between 9 and 10. This convergence is firmly supported by the observation that the stationary density function peaks precisely at 9.0846, as clearly illustrated in Figure 6b. Ultimately, these transition pathways offer a deeper understanding of the system's behavior, effectively validating the predicted dynamics.

The rising rate of the two trajectories of $X_m$ initiating from 0.0001 and 1 in Figure 5a differs significantly from that of the two trajectories of $X_m$ commencing from 0.001 and 4 in Figure 6a. While the peak heights of the probability density function in Figure 5b are different from those in Figure 6b, the locations of the peaks are surprisingly consistent, all precisely at 9.0846. We compare the peak heights of the probability density function while noting the surprising consistency in the location of the peaks.

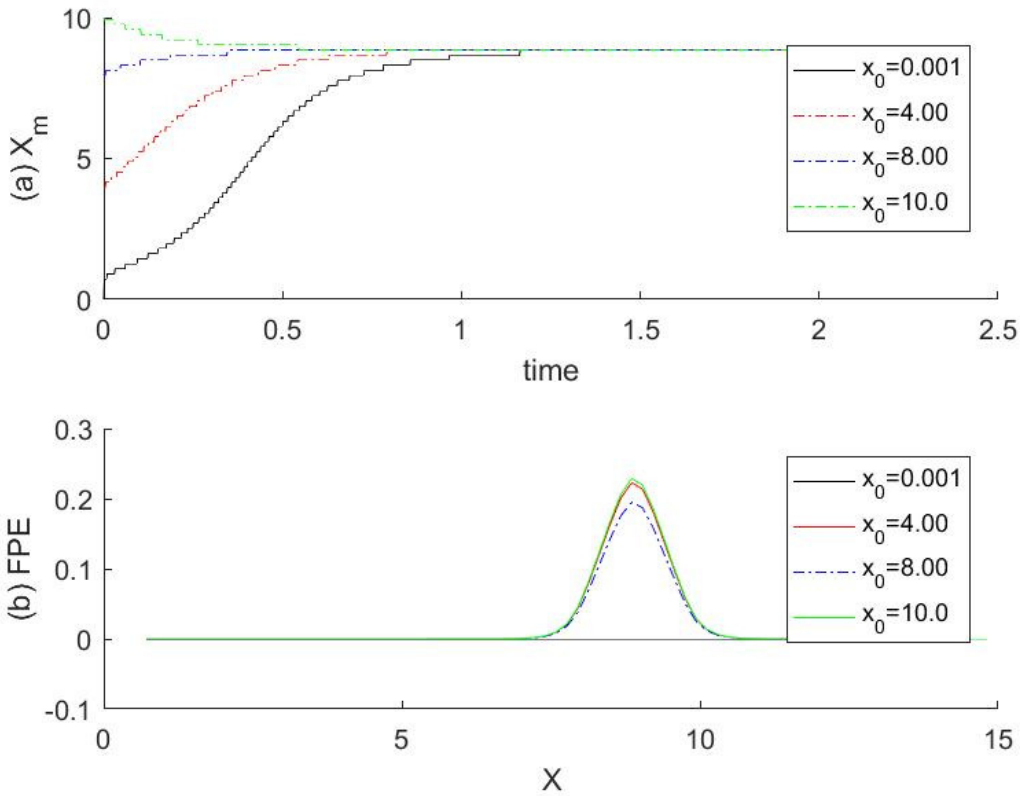


**Figure 6.** (**a**) Most probable orbits and most probable equilibrium states for System (1) with equilibrium state $X_m$ between 9 and 10. For the initial condition $x_0$, there is one value (0.001) which is less than $X_2$, two values (4 and 8) between $X_2$ and $X_3$, and one value (10) which is greater than $X_3$. (**b**) The solution of the FPE of Model (1). The stationary density function of the FPE has maximum value at the equilibrium state $X_m$. The other parameters are fixed: $s = 1$, $\gamma_2 = 0.1$, $\gamma_3 = 2.67$, $\gamma_4 = 1$, $\alpha = 1.5$, $\epsilon = 0.5$, $\beta = 0.27 < 1$, $\lambda = 0$, and $x_0 \in (0, 10]$. The bifurcation time is 1.2.

## 6. Conclusions

In the present work, we have studied the Onsager–Machlup functional and the most probable phase portraits of the stochastic growth Model (1) for a single-species population with strong Allee effects driven by Lévy noise, focusing on the effect of different values for the initial condition on the MPPP of the nonlinear dynamical system. We have observed the dynamic changes in the biological System (1) over time by simulating responses to perturbations or interventions as well as capturing natural fluctuations. Small disturbances may cause a transition between the extinction stable state $X_1$ and the upper equilibrium state $X_3$. Thus, we have been able to develop a deterministic quantity, namely, the maximally likely trajectory, to analyze the transition phenomena in a stochastic jump environment.

In order to find the most likely pathways in transition phenomena, we have calculated the most probable paths of the stochastic differential Equation (1) using the stationary density function of the nonlocal Fokker–Planck equation associated with a nonlocal partial differential equation. We have investigated the impact of the deterministic parameters, noise intensities, and domain size on the FPE. In addition, we have studied the dependence of the probability density on the initial condition $x_0$. Our findings demonstrate that the maximum of the stationary density function is positioned at the most probable stable equilibrium state $X_m$.

In conclusion, Model (1) shows good performance in predicting biological processes. Its accuracy and reproducibility ensure that it will continue to contribute to future research and a deeper understanding of biological systems. The most probable path has been used as

a reliable and informative indicator that can assist in understanding the stochastic dynamics of the single-species Model (1) based on the evolution of the probability density function over time. Evaluating the biological relevance and validation of our modeling approach has involved assessing the model's ability to accurately represent biological processes, comparing its predictions with numerical data, and ensuring its robustness and predictive power. By considering these aspects, the modeling approach has proven to be effective in enhancing our understanding of biological systems. This has been clearly documented, enabling others to extend the work.

**Author Contributions:** Conceptualization, D.T.; Methodology, S.Y.; Software, S.Y.; Validation, A.T.A.; Formal analysis, A.T.A.; Investigation, S.Y.; Resources, J.B.; Data curation, D.T.; Writing—original draft, A.T.A.; Writing—review & editing, S.Y.; Visualization, A.T.A.; Supervision, J.B. All authors have read and agreed to the published version of the manuscript.

**Funding:** This research received no external funding.

**Data Availability Statement:** Numerical algorithms and source code that support the findings of this study are openly available on GitHub; see, Ref. [42].

**Conflicts of Interest:** The authors declare no conflicts of interest.

## References

1. Zhang, Y.; Lv, J.; Zou, X. Dynamics of stochastic single-species models. *Math. Methods Appl. Sci.* **2020**, *43*, 8728–8735. [CrossRef]
2. Allen, L.J. *An Introduction to Stochastic Processes with Applications to Biology*; CRC Press: Boca Raton, FL, USA, 2010.
3. Dennis, B. Allee effects: Population growth, critical density, and the chance of extinction. *Nat. Resour. Model.* **1989**, *3*, 481–538. [CrossRef]
4. Dennis, B.; Assas, L.; Elaydi, S.; Kwessi, E.; Livadiotis, G. Allee effects and resilience in stochastic populations. *Theor. Ecol.* **2016**, *9*, 323–335. [CrossRef]
5. Lo, C.F. Stochastic Gompertz model of tumour cell growth. *J. Theor. Biol.* **2007**, *248*, 317–321. [CrossRef]
6. Liu, M.; Bai, C. A remark on a stochastic logistic model with Lévy jumps. *Appl. Math. Comput.* **2015**, *251*, 521–526. [CrossRef]
7. Guiot, C.; Delsanto, P.P.; Carpinteri, A.; Pugno, N.; Mansury, Y.; Deisboeck, T.S. The dynamic evolution of the power exponent in a universal growth model of tumors. *J. Theor. Biol.* **2006**, *240*, 459–463. [CrossRef] [PubMed]
8. Baratti, R.; Alvarez, J.; Tronci, S.; Grosso, M.; Schaum, A. Characterization with Fokker-Planck theory of the nonlinear stochastic dynamics of a class of two-state continuous bioreactors. *J. Process Control* **2021**, *102*, 66–84. [CrossRef]
9. Zhang, X.; Wang, K. Stability analysis of a stochastic Gilpin-Ayala model driven by Lévy noise. *Commun. Nonlinear Sci. Numer. Simul.* **2014**, *19*, 1391–1399. [CrossRef]
10. Noor, A.; Barnawi, A.; Nour, R.; Assiri, A.; El-Beltagy, M. Analysis of the stochastic population modelwith random parameters. *Entropy* **2020**, *22*, 562. [CrossRef]
11. Braumann, C. *Introduction to Stochastic Differential Equations with Applications to Modelling in Biology and Finance*; John Wiley & Sons: Hoboken, NJ, USA, 2019.
12. Sun, Z.; Lv, J.; Zou, X. Dynamical analysis on two stochastic single-species models. *Appl. Math. Lett.* **2020**, *99*, 105982. [CrossRef]
13. Elaydi, S.; Sacker, R.J. Population models with Allee effect: A new model. *J. Biol. Dynam.* **2010**, *4*, 397–408. [CrossRef] [PubMed]
14. Krstić, M.; Jovanović, M. On stochastic population model with the Allee effect. *Math. Comput. Model.* **2010**, *52*, 370–379. [CrossRef]
15. Yang, Q.; Jiang, D. A note on asymptotic behaviors of stochastic population model with Allee effect. *Appl. Math. Model.* **2011**, *35*, 4611–4619. [CrossRef]
16. Mao, X.; Marion, G.; Renshaw, E. Environmental Brownian noise suppresses explosions in population dynamics. *Stoch. Proc. Appl.* **2002**, *97*, 95–110. [CrossRef]
17. Yuan, S.; Li, Y.; Zeng, Z. Stochastic bifurcations and tipping phenomena of insect outbreak systems driven by $\alpha$-stable Lévy processes. *Math. Model. Nat. Phenom.* **2022**, *17*, 34. [CrossRef]
18. Yuan, S.; Blömker, D.; Duan, J. Stochastic turbulence for Burgers equation driven by cylindrical Lévy process. *Stoch. Dynam.* **2022**, *22*, 2240004. [CrossRef]
19. Yuan, S.; Zeng, Z.; Duan, J. Stochastic bifurcation for two-time-scale dynamical system with $\alpha$-stable Lévy noise. *J. Stat. Mech. Theory E* **2021**, *2021*, 033204. [CrossRef]
20. Yuan, S.; Wang, Z. Bifurcation and chaotic behavior in stochastic Rosenzweig–MacArthur prey–predator model with non-Gaussian stable Lévy noise. *Int. J. Nonlin. Mech.* **2023**, *150*, 104339. [CrossRef]
21. Rahmani, D.; Saraj, M. The logistic modeling population: Having harvesting factor. *Yugosl. J. Oper. Res.* **2015**, *25*, 107–115. [CrossRef]
22. Tesfay, A.; Tesfay, D.; Brannan, J.; Duan, J. A logistic-harvest model with Allee effect under multiplicative noise. *Stoch. Dynam.* **2021**, *21*, 2150044. [CrossRef]

23. Tesfay, A.; Tesfay, D.; Yuan, S.; Brannan, J.; Duan, J. Stochastic bifurcation in single-species model induced by $\alpha$-stable Lévy noise. *J. Stat. Mech. Theory E* **2021**, *2021*, 103403. [CrossRef]
24. Goel, N.S.; Richter-Dyn, N. *Stochastic Models in Biology*; Elsevier: New York, NY, USA, 2013.
25. Lande, R.; Engen, S.; Saether, B.E. *Stochastic Population Dynamics in Ecology and Conservation*; Oxford University Press: New York, NY, USA, 2003.
26. Wilkinson, D.J. *Stochastic Modelling for Systems Biology*; Chapman and Hall/CRC: Boca Raton, FL, USA, 2018.
27. Wu, R.; Zou, X.; Wang, K. Dynamics of logistic system driven by Lévy noise under regime switching. *Electron. J. Differ. Equ.* **2014**, *2014*, 1–16.
28. Humphries, N.; Queiroz, N.; Dyer, J.R.; Pade, N.G.; Musyl, M.K.; Schaefer, K.M.; Sims, D.W. Environmental context explains Lévy and Brownian movement patterns of marine predators. *Nature* **2010**, *465*, 1066–1069. [CrossRef]
29. Yuan, S.; Blömker, D. Modulation and amplitude equations on bounded domains for nonlinear SPDEs driven by cylindrical $\alpha$-stable Lévy processes. *SIAM J. Appl. Dyn. Syst.* **2022**, *21*, 1748–1777. [CrossRef]
30. Koren, T.; Chechkin, A.; Klafter, J. On the first passage time and leapover properties of Lévy mmotion. *Physica A* **2007**, *379*, 10–22. [CrossRef]
31. Duan, J. *An Introduction to Stochastic Dynamics*; Cambridge University Press: New York, NY, USA, 2015.
32. Cheng, Z.; Duan, J.; Wang, L. Most probable dynamics of some nonlinear systems under noisy fluctuations. *Commun. Nonlinear Sci. Numer. Simul.* **2016**, *30*, 108–114. [CrossRef]
33. Wang, H.; Chen, X.; Duan, J. A stochastic pitchfork bifurcation in most probable phase portraits. *Int. J. Bifurc. Chaos* **2018**, *28*, 1850017. [CrossRef]
34. Han, P.; Xu, W.; Wang, L.; Zhang, H.; Ma, S. Most probable dynamics of the tumor growth model with immune surveillance under cross-correlated noises. *Physica A* **2020**, *547*, 123833. [CrossRef]
35. Onsager, L.; Machlup, S. Fluctuations and irreversible processes. *Phys. Rev.* **1953**, *91*, 1505. [CrossRef]
36. Chao, Y.; Duan, J. The onsager-machlup function as lagrangian for the most probable path of a jump-diffusion process. *Nonlinearity* **2019**, *32*, 3715. [CrossRef]
37. Cheng, X.; Wang, H.; Wang, X.; Duan, J.; Li, X. Most probable transition pathways and maximal likely trajectories in a genetic regulatory system. *Physica A* **2019**, *531*, 121779. [CrossRef]
38. Jin, Y. Analysis of a stochastic single species model with Allee effect and jump-diffusion. *Adv. Differ. Equ.* **2020**, *2020*, 165. [CrossRef]
39. Gao, T.; Duan, J.; Li, X. Fokker-planck equations for stochastic dynamical systems with symmetric Lévy motions. *Appl. Math. Comput.* **2016**, *278*, 1–20. [CrossRef]
40. Huang, Y.; Chao, Y.; Yuan, S.; Duan, J. Characterization of the most probable transition paths of stochastic dynamical systems with stable Lévy noise. *J. Stat. Mech. Theory E.* **2019**, *2019*, 063204. [CrossRef]
41. Yuan, S.; Hu, J.; Liu, X.; Duan, J. Slow manifolds for dynamical systems with non-Gaussian stable Lévy noise. *Anal. Appl.* **2019**, *17*, 477–511. [CrossRef]
42. Yuan, S. Code. Github. 2024. Available online: https://github.com/shenglanyuan/most-probable-dynamics-of-the-single-species-with-allee-effect-under-jump-diffusion-noise (accessed on 28 April 2024).